International Journal of Biological Macromolecules 178 (2021) 121–135

Contents lists available at ScienceDirect

International Journal of Biological Macromolecules

journal homepage: http://www.elsevier.com/locate/ijbiomac

Radioprotective effects of *Cryptosporidium parvum* lysates on normal cells

Pankaj Kumar Chaturvedi [a], Enkhsaikhan Erdenetuya [a], D.S. Prabakaran [a], Chang-Gok Woo [b], Ki-Hwan Kim [c], Jae-Ran Yu [d], Woo-Yoon Park [a,*]

[a] Department of Radiation Oncology, Chungbuk National University Hospital, Chungbuk National University College of Medicine, Cheongju 28644, Republic of Korea
[b] Department of Pathology, Chungbuk National University Hospital, Chungbuk National University College of Medicine, Cheongju 28644, Republic of Korea
[c] Department of Radiation Oncology, Chungnam National University Hospital, Daejeon 35015, Republic of Korea
[d] Department of Environmental and Tropical Medicine, Konkuk University College of Medicine, Chungju 27478, Republic of Korea

ARTICLE INFO

Article history:
Received 7 December 2020
Received in revised form 14 February 2021
Accepted 20 February 2021
Available online 23 February 2021

Keywords:
Cryptosporidium parvum lysates
Radioprotection
ROS
DNA damage repair
Normal cells

ABSTRACT

Two fractions, small and big (CpL-S, CpL-B), from *Cryptosporidium parvum* lysate (CpL) were prepared and its radioprotective activity was evaluated on normal cells. Both fractions improved cell viability of normal cells in a dose-dependent manner. 20 μg CpL-S and CpL-B improved cell viability of 10 Gy irradiated COS-7 cells by 38% and 34% respectively, while in HaCat cells 16% and 18% improved cell viability was observed, respectively. CpL-S scavenged IR-induced ROS more effectively compared to the CpL-B, 50% more in COS-7 cells and 15% more in HaCat cells. There was a significant reduction of γH2AX, Rad51, and pDNA-PKcs foci in CpL-S treated cells compared to control or CpL-B group at an early time point as well as late time point. In 3D skin tissue, CpL-S reduced the number of γH2AX positive cells by 31%, compared to control, while CpL-B reduced by 9% ($p < 0.005$) at 1 h post 10 Gy irradiation and 22% vs 6% at 24 h post-IR ($p < 0.005$). Taken together, CpL-S significantly improved cell viability and prevented radiation-induced DNA damage in normal cells as well as 3D skin tissues by effectively scavenging ROS generated by ionizing radiation. CpL-S can be a candidate for radioprotector development.

1. Introduction

Radiation therapy (RT) is one of the principal methodologies to eradicate or control malignant diseases. In developed countries, more than half of all cancer patients receive some form of RT during their oncologic treatment [1]. However, normal tissue toxicity is a noteworthy dose-limiting aspect for the cure with RT, which adversely affects a patient's life quality throughout and post-RT. Conversely, reductions in radiation dose or treatment delays may lead to poor therapeutic outcomes. Thus, the normal tissue protection from radiation-induced injury remains a critical RT goal [1].

Nucleic acids are believed to be the critical target of ionizing radiation (IR). IR damages DNA through two processes, direct and indirect actions. When radiation directly interacts with DNA and causes structural changes like DNA strand breaks, point mutations, chromosome aberrations, DNA crosslinks, etc., it is known as direct action [2]. If not repaired, these modifications can initiate signal cascades leading to cell death. Direct action is predominantly the cell-killing mode following high linear energy transfer radiation (LET) (i.e., α-particles and neutrons). DNA lesions following these densely IRs, are challenging to repair and thus more difficult to modify by the pharmacological interventions [1].

On the other hand, the generation of highly reactive and chemically unstable free radicals accounts for indirect actions. These radicals interact with DNA and often lead to severe consequences [3]. Most of the radiation damage caused by indirect action occurs due to radiolysis of water, which is present in abundant quantity inside the cells. Radiolysis is a process in which the IR ionizes water molecules and generates several forms of free radicals. In particular, hydroxyl radicals are of great significance as they are highly reactive and have great potential to interact with DNA and cause structural changes [4]. Hydroxyl radicals account for 2/3rd of radiation-induced cell damage following low LET radiations (like X-rays or γ-rays), which makes indirect action the predominant cell-killing mode [2]. However, cellular damages caused by indirect action have the potential to be neutralized by the intervention of free radical scavengers or antioxidants [1].

Swift and extensive phosphorylation of histone H2A serine (H2AX variant) to create γH2AX is the earliest mark of DNA double-strand breaks (DSBs) [5,6]. Hence, γH2AX expression is regarded as a sensitive indicator of DNA DSBs induced by IR [7]. IR is an exogenous genotoxic agent, which can prompt reactive oxygen species (ROS) production in cells [8]. Usually, the cells exposed to IR have elevated intracellular ROS levels. This condition affects the normal state of DNA and other cellular components like membrane proteins and lipids [9]. ROS-induced DNA DSBs have direct impact on cell survival [10]. There are reports

* Corresponding author at: Department of Radiation Oncology, Chungbuk National University Hospital, Chungbuk National University College of Medicine, Chungdae-ro 1, Seowon-gu, Cheongju 28644, Republic of Korea.
E-mail address: wynpark@chungbuk.ac.kr (W.-Y. Park).

https://doi.org/10.1016/j.ijbiomac.2021.02.151
0141-8130/

which suggest that the eukaryotic cells with DSBs engage a DNA damage response pathway to arrest the cell cycle until DNA damage is repaired or initiate cell death if it is impossible to repair DNA damage [11]. During this stage, H2AX at the DNA damage site is rapidly phosphorylated, giving rise to γH2AX, where several molecules associated with DNA repair or apoptosis assemble and give rise to IR-induced foci [12].

Researchers have proposed various agents to modulate the cell damages associated with IR exposure, e.g., glutathione-elevating compounds or antioxidants may reduce DNA damage and theoretically lessen post-radiation chances of carcinogenesis [13,14]. Several radioprotectors with marked radioprotective activity are available, e.g., *N*-acetylcysteine, Vitamin C, Curcumin, Green Tea extracts, Amifostine, Palifermin, to name a few. However, the available literature does not suggest that they can prevent long-term stochastic effects of radiation exposure [15]. Although many researchers have reported several potential radioprotective agents, there are currently very few of them approved for clinical use. Amifostine and Palifermin are two well-known US Food and Drug Administration (USFDA) approved agents. However, due to side effects and toxicity, Amifostine usage in clinical nuclear/radiological exposure settings failed [16]. Thus, there is an increasing urge to develop new radioprotectors and carry out long-term research to establish the clinical value of radioprotective agents.

Daly et al. demonstrated that the protein-free ultrafiltered preparation of *Deinococcus radiodurans* (a highly radio-resistant bacteria) extracts prevented protein oxidation at the high doses of IR. Such extracts also effectively protected *Escherichia coli* (*E. coli*) and human Jurkat T-cells from the damage induced by IR. In contrast, such preparations from radiosensitive bacteria were not radioprotective. The authors rationally designed a radioprotective Mn^{2+}-decapeptide (MDP) complex from the protein-free ultrafiltrates of *D. radiodurans* [17]. Further Gupta et al. [18] reported that all mice treated with this complex survived exposure to 9.5 Gy irradiation. However, MDP complex was shown to specifically protect protein from IR-induced damage, but not DNA/RNA [19]. *Cryptosporidium parvum* (*C. parvum*), an obligate intracellular protozoan, infects a wide range of vertebrates, which includes humans and animals [20]. C. parvum (Iowa isolate II) genome is 9.1 megabase pairs long and contains 4020 genes out of which 3941 are protein coding genes. The protein size ranges from 49 amino acids in length to 13,413 amino acids (cryptodb.org). Previously we have shown that among parasites, *C. parvum* exhibited the highest known resistance for γ-irradiation for the first time. It was necessary to irradiate with 50 kGy to eliminate *C. parvum* infectivity in mice [21]. Also, we have reported that recombinant thioredoxin peroxidase-like protein (22 kDa) from *C. parvum* (CpTPX) conferred radioprotection to COS-7 cells from up to 8 Gy of IR. The survival rates were 12–22% higher in CpTPx group at 72 h after 8 Gy irradiation compared to CmTPx (*C. muris* thioredoxin peroxidase; *C. muris* is radiosensitive) or control group [8]. We believe in addition to thioredoxin peroxidase (TPx), there may be many more bioactive components which help *C. parvum* to endure high doses of ionizing radiation. The ability of *C. parvum* to survive high doses of ionizing radiation and the ability of its bioactive molecules to confer radioprotection to normal cells makes it an excellent candidate to exploit it in the studies related to radioprotectors development. Thus with an idea to separate big molecules (more than 10 kDa) like thioredoxin peroxidase or superoxide dismutase (SOD) etc. from smaller molecules (less than 10 kDa) comprising of very small proteins, short peptides or free amino acids, we prepared *C. parvum* lysate (CpL) and subjected it to filtration by centrifugal filters with molecular weight cut off (MWCO) of 10 kDa to evaluate their radioprotective activity on normal cells and 3D skin tissue.

2. Material and methods

2.1. C. parvum lysate (CpL) preparation

CpL was prepared as described earlier [22], with slight modifications. Live *C. parvum* oocysts (Iowa isolate from experimentally infected calves) were purchased from Waterborne Inc. (New Orleans, LA, USA). Each vial contains 5.0×10^8 live oocysts. The oocysts were lysed to prepare lysates within one month of receiving them. The oocyst stock was gently vortexed, and 2.5×10^8 oocysts were taken out in microcentrifuge tubes. The tubes containing oocysts were subjected to centrifuge at 2500 ×*g* for 5 min at 4 °C. The supernatant was discarded carefully without disturbing the pellet. The pellet was then re-suspended in 1.6 ml phosphate buffer saline (PBS) pH 7.2, supplemented with 1× complete protease inhibitor cocktail (#11873580001, Roche, Mannheim, Germany). The oocyst wall was loosened by 5 cycles of freezing (2 min each) in liquid nitrogen and thawing at room temperature (10 min each). The sample was cooled on ice for 10 min before sonication. To break the oocyst membrane and release the proteins, 30 cycles of ultrasonication (VirSonic 3000 Sonicator Cell Disruptor Dismembrator from Misonix, Farmingdale, NY, USA) was performed on ice as follows: 5 s sonication at level 10 followed by a resting time of 55 s. The sample was cooled down on ice for 10 min and then centrifuged at 10,000 ×*g* for 5 min at 4 °C to sediment the debris. After centrifugation, the supernatant was collected in a fresh microcentrifuge tube. Further, the CpL was filtered using Amicon ultra-4 10K centrifugal filter device (#UFC801024, Merck Millipore, Billerica, MA, USA) in a cooling centrifuge equipped with swing bucket rotor 4000 ×*g*, 4 °C, for 30 min or until 200 μl volume of retentate was remaining in the filtration device. After centrifugation 2 fractions were obtained: retentate and filtrate. Filtrate comprised of small molecules <10 kDa in size (CpL-S) and retentate composed of big molecules >10 kDa in size (CpL-B). Post filtration the fractions were collected in new microcentrifuge tubes. On an average the recovery volume for CpL-S was 1.35 ml and CpL-B was 0.2 ml. The volume of CpL-B was adjusted to 1.35 ml with PBS pH 7.2. Then the fractions were subjected to protein estimation by Bradford assay. Average concentration of CpL-S was 0.65 mg/ml and CpL-B was 1.8 mg/ml. Finally, concentration of both the fractions were adjusted to 0.5 mg/ml by PBS, pH 7.2. The fractions were aliquot in small volumes of 350 μl each and stored in deep freezer (−70 °C) until use.

2.2. Cell lines and 3D skin tissue

Two normal cell lines (COS-7 and HaCat) and 3D skin (Neoderm®-ED) were used in the present study. HaCat cell line (human keratinocyte) was purchased from AddexBio (#T0020001, San Diego, CA, USA), and COS-7 cell line (derived from the African green monkey kidney) was procured from the Korean Cell Line Bank (KCLB No. 21651, Seoul, Korea). Both the cell lines are normal cell lines immortalized by SV40 transfection. The cells were maintained as a monolayer culture in 5% CO_2 and humidified environment at 37 °C in Dulbecco's Modified Eagle's Medium (DMEM, #LM001-05, Welgene, Daegu, Korea) supplemented with 10% fetal bovine serum (FBS, #S001-07, Welgene), 100 U/ml penicillin and 100 μg/ml streptomycin (#LS202-02, Welgene). The cells were routinely passaged by phenol red free trypsin-EDTA solution (#LS015-08, Welgene), at 80–90% confluency. Neoderm®-ED is a reconstituted human skin equivalent model, obtained commercially from Tego Science (Seoul, Korea) and cultured as described by the manufacturer. The Neoderm® 3D skin tissues were cultured in 12 well plates containing maintenance media (provided by the manufacturer) at 37 °C, with 5% CO_2 and ambient humidity. The media was replaced every two days.

2.3. Cell viability assay

Cell viability was assessed using a modified colorimetric technique based on live cells' ability to reduce water soluble tetrazolium salt (WST-1; (4-[3-(4-iodophenyl)-2-(4-nitro-phenyl)-2H-5-tetrazolio]-1,3-benzene sulfonate)) into formazan with the help of mitochondrial reductases. Briefly, 5.0×10^3 exponentially growing cells were seeded in 100 μl media per well, in triplicate in 96-well plates (#30096, SPL

Life Sciences, Pocheon, Gyeonggi-do, Korea) and allowed to attach overnight. The old media was aspirated and the cells were then treated with various quantities of CpL (0, 5, 10 and 20 μg) supplemented in 100 μl serum-free media for 24 h. At the end of the treatment, cells were washed with Dulbecco's phosphate-buffered saline, pH 7.5 (D-PBS, #LB 001-02 Welgene) and fresh complete growth DMEM supplemented with HEPES (#LM001-10, Welgene) was added to each well. Then the cells were exposed to IR of 2 or 10 Gy (by a single beam of 6 MV) using a medical linear accelerator (ONCOR expression, Siemens, CA, USA). Un-irradiated cells served as control. The cells were allowed to grow for 48 h before performing the MTT assay. For measuring cell viability, 10 μl of EZ-Cytox (DoGen Bio Co. Ltd, Seoul, Korea) was added to each well and incubated at 37 °C for 1 h. Subsequently, the absorbance was recorded using a microplate reader at 450 nm (iMark microplate reader, Biorad, Hercules, CA, USA). The cell viability was expressed as a percentage of the cells' absorbance treated with CpL filtrates relative to control cells.

2.4. ROS detection by confocal imaging (CellRox® Green)

5.0×10^4 cells were grown on coverslips (#0111520, Paul Merienfeld Gmbh, Germany) in 4 well plates (#30004, SPL Life Sciences) and treated for 24 h with 0 or 20 μg CpL in 250 μl serum free media. At the end of the filtrate treatment, the cells were rinsed with 1× D-PBS (#LB 001-02 Welgene) devoid of phenol red, Ca^{2+} and Mg^{2+}, added 5 μM of CellRox® green (#C10444, Molecular Probes, Invitrogen, Eugene, OR, USA) along with NucBlue™ (#R37605, Molecular Probes, Invitrogen) live cell stain, two drops per ml of media and incubated at 37 °C for 30 min in the dark. The cells were rinsed with 1× D-PBS and supplied with HEPES supplemented DMEM (#LM001-10, Welgene). The cells were irradiated with 0 Gy or 10 Gy as described above and fixed with 2% paraformaldehyde (#J19943-K2, Thermo Scientific, Geel, Belgium). After washing the cells with D-PBS, coverslips were mounted on slides (#1000612, Paul Merienfeld Gmbh, Germany) using the Dako fluorescence mounting medium (#S3023, Dako, CA, USA) and dried overnight in the dark. Images were captured within 24 h and analyzed using a confocal laser scanning microscope (#LSM-880, Carl Zeiss Microscopy, LLC, White Plains, NY, USA). The images were thresholded, and fluorescence intensities of at least 50 cells from each panel were calculated using ImageJ software, National Institute of Health (NIH, Bethesda, MD, USA, https://imagej.nih.gov/ij). Briefly, the two channels of confocal images were separated by ImageJ software and the green channel image was converted to 16-bit file. A duplicate image was created and auto-thresholded. Adjusted the threshold lower value by 1 or 2 points so that all the cells were identified by the software. Chose grayscale image and analyzed it for particles.

2.5. Immunofluorescence

Cells were grown on coverslips placed in 4 well plates as described above and treated with or without 20 μg of CpL in 250 μl serum free media per well for 24 h. At the end of the CpL treatment, the cells were exposed to 0 or 10 Gy of IR at room temperature. After incubation for the indicated periods, the cells were fixed with 2% paraformaldehyde (Thermo Scientific) in PBS and then permeabilized with 0.1% Triton X-100 (#0694-1L, Amresco, Solon, OH, USA) and blocked with 10% FBS (#S001-07, Welgene) for 30 min, followed by incubation with primary antibodies anti-γH2AX (#05-636, EMD Millipore, Temecula, CA, USA), anti-Rad51 (#ab133534, Abcam, Cambridge, MA, USA) and anti-pDNA-PKcs (#ab18192 Abcam) at a dilution of 1:500 in 2% FBS/PBS overnight at 4 °C. The cells were further incubated with Alexa488 or Alexa594 conjugated secondary antibodies at a dilution of 1:1000 (#A11001, or A11072, Invitrogen, Carlsbad, CA, USA) for 1 h. Nuclei were stained with 1 μg/ml of DAPI (#D8417, Sigma, St. Louis, MO, USA). The coverslips were mounted on slides as described in the previous section. Random images were captured with the help of confocal laser scanning microscope (#LSM-880, Carl Zeiss Microscopy), and foci were counted in at least 50 cells from each group, with the help of Cellprofiler software, an open-source software for measuring and analyzing cell images [23].

2.6. Immunohistochemistry

3D human skin model Neoderm®-ED were transferred in 12 well plates containing growth media provided by the manufacturer and grown overnight at 37 °C, 5% CO_2 in a humidified chamber. The next morning 0 or 40 μg of CpL-S/CpL-B was directly added onto the top of skin cultures drop by drop. Untreated cultures served as control. Twenty-four hours later, the media was replaced with a fresh one, and the skin cultures were subjected to 0 or 10 Gy of IR at room temperature. The skin samples were collected at 1 h or 24 h post-IR, fixed in formalin, and embedded in paraffin blocks. Immunohistochemistry (IHC) of the paraffin sections was performed using a Benchmark automatic immunostaining device (Ventana Medical Systems, Tucson, AZ, USA). Briefly, 4 μm thick sections were mounted on silanized slides and allowed to dry for 10 min at room temperature. The slides were then deparaffinized, rehydrated, and antigen retrieval was done before staining. The slides were then processed for hematoxylin and eosin (H&E) staining or incubated with primary antibodies against γH2AX (#05-636, EMD Millipore) followed by HRP-conjugated secondary antibody (#7076S Cell Signaling Tech. Inc., Danvers, MA, USA). Antigen was visualized with substrate chromogen 3,3′ diaminobenzidine (#K3468, Dako liquid DAB chromogen; Dako, Carpinteria, CA, USA). Finally, tissue specimens were counterstained with hematoxylin (Hematoxylin QS #H-3404; Vector Laboratories, Burlingame, CA, USA) for 20 s to distinguish the nucleus from the cytoplasm. Slides were dried in the dark, and random images were captured with the help of Olympus IX71 microscope (40× objective) coupled with Olympus CellSens Standard 2.3 software (Olympus, Shinjuku, Tokyo, Japan). Cells positive for γH2AX expression were counted manually using ImageJ software (NIH), in 3 sections (each having at least 100 cells) from each group.

2.7. Statistical analysis

All data are presented as the mean of 3 independent experiments. Differences among the groups were calculated by two-way ANOVA (analysis of variance) followed by post hoc Tukey multiple comparison tests, performed using GraphPad Prism version 8.4.3 for Windows (GraphPad Software, La Jolla, CA USA, www.graphpad.com). p-Value ≤ 0.05 was considered to be statistically significant.

3. Results

3.1. CpL protects COS-7 and HaCat cells from radiation-induced cell death

Before performing cell viability assay, the toxicity of various doses of CpL was checked in COS-7 cells. It was observed that treatment with 20 μg of CpL for 3 h made the cells stressful. Morphological changes and some debris could be seen easily under the microscope. However, after 23 h, the cells recovered and appeared healthy when observed under the microscope (Fig. S1). Cell viability assay was performed using a water-soluble tetrazolium (WST) based MTT assay kit (EZ-Cytox). MTT assay showed that CpL improved cell viability of COS-7 cells and HaCat cells at 2 Gy and 10 Gy compared to control cells. Both the fractions had similar effects on cell viability (Fig. 1). A dose-dependent increase in cell viability was evident in CpL treated group in both the cell lines. In the case of COS-7 cells, the CpL-S improved cell viability of 10 Gy group, from 65.9% ± 3.8 (IR alone) to 93.3% ± 4.6 (IR + 20 μg CpL-S) (Fig. 1A), while the CpL-B also enhanced cell viability approximately by the same extent, 68.4% ± 2.6 (IR alone) vs 92.5% ± 4.5 (IR + 20 μg CpL-B) (Fig. 1B). Interestingly, COS-7 cells exposed to 2 Gy irradiation recovered completely in

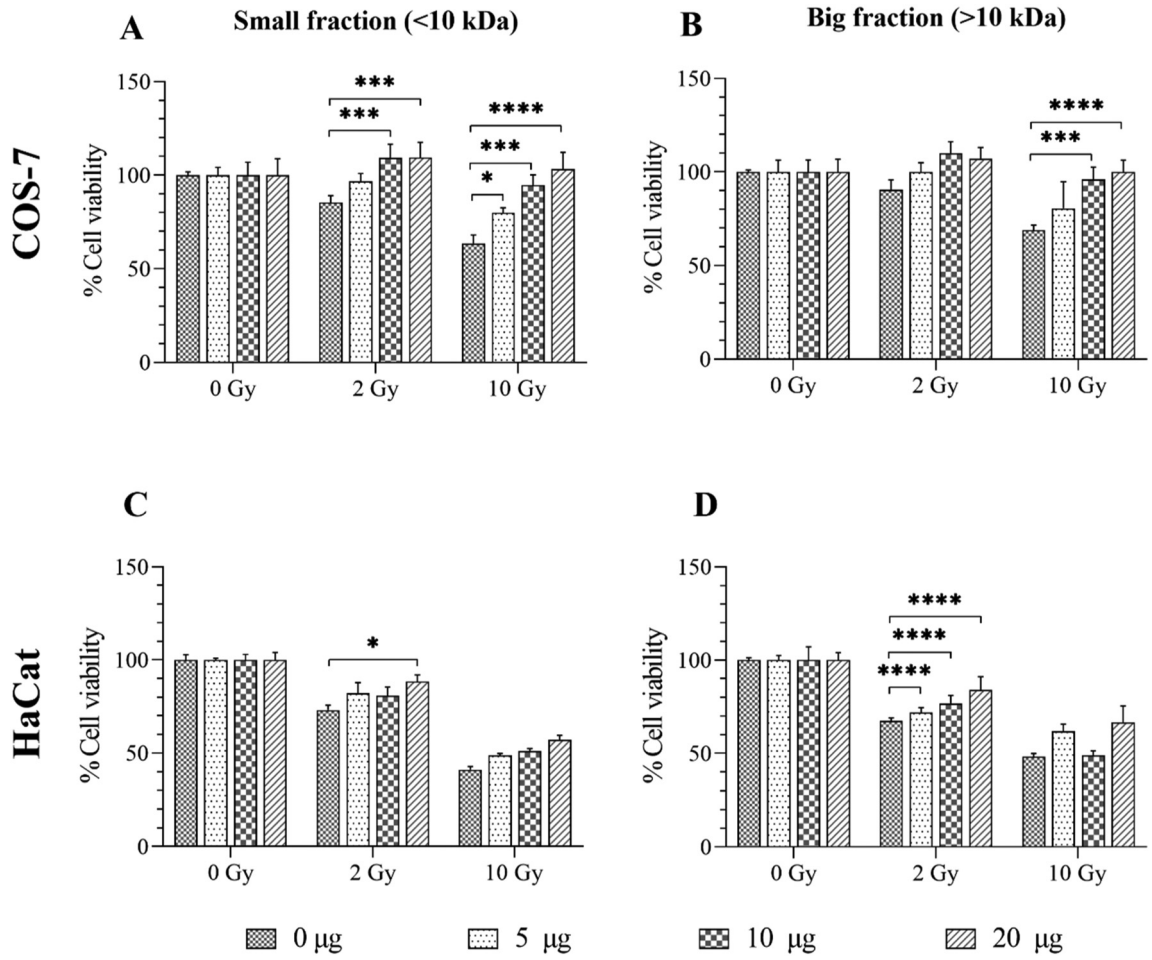

Fig. 1. Dose dependent change in survival of cells treated with two fractions of CpL. COS-7 and HaCat cells were treated with CpL (0, 5, 10 and 20 μg). After 24 h, cells were irradiated with 0, 2 or 10 Gy of IR. Cell viability was measured by MTT assay, 48 h post-irradiation. COS-7 cells treated with CpL-S (A) and CpL-B (B); HaCat cells treated with CpL-S (C) and CpL-B (D). Data represents average of 3 experiments (the data has been normalized to control) and error bars represent ± standard error of means. p-Values of statistically significant differences are shown. *$p < 0.05$, ***$p < 0.0005$; ****$p < 0.0001$.

10 μg and 20 μg groups of both the fractions (Fig. 1A and B). In HaCat cells, the amplitude of improvement in cell viability was lower as compared to COS-7 cells. At 10 Gy the CpL-S treated cells showed cell viabilities of 41.2% ± 1.6 (IR alone) vs 57.2 ± 2.5 (IR + 20 μg CpL-S) (Fig. 1C), while the CpL-B showed 48.31% ± 1.7 (IR alone) vs 66.7% ± 8.8 (IR + 20 μg CpL-B) (Fig. 1D). The cells irradiated with 2 Gy also had shown similar improvement in the cell viability (Fig. 1C and D); however, almost 100% viability was not achieved, unlike COS-7 cells.

3.2. CpL scavenges ROS generated by IR in both the normal cells

We analyzed the ROS by confocal imaging using a photo-stable dye CellROX® green. After fixing the cells on the slide, images were captured randomly, and fluorescence intensity was quantified from at least 50 cells using ImageJ software (NIH). In COS-7 (Fig. 2A) and HaCat cells (Fig. 2B), it can be seen clearly that the cells exposed to 10 Gy IR have the highest fluorescence, which seems to have reduced in CpL treated cells. It was observed that in COS-7 cells, the ROS levels shot up to 168.8% as compared to the control group, which was alleviated to 104.9% ($p < 0.005$) by CpL-S and 155.74% by CpL-B (Fig. 2C). Similarly, in HaCat cells, ROS accumulated up to 218% in 10 Gy irradiated cells compared to control (Fig. 2D). Both the fractions showed significant reduction in ROS level, 107.1% by CpL-S ($p < 0.0001$) and 122.6% by CpL-B ($p < 0.0005$).

3.3. CpL reduces the expression of DNA damage marker γH2AX

Random images were captured with the help of a confocal microscope (LSM-880, Zeiss) at 40× objective and 2× digital zoom. IR exposed cells accumulated a lot of γH2AX foci at the DSBs sites, which were reduced due to the intervention of CpL in both the cell lines at 1 h as well as 24 h post-IR. A basal level expression of γH2AX can also be visualized in the un-irradiated cells (Fig. 3A, B). It was found that the COS-7 cells (Fig. 3C) exposed to 10 Gy IR have accumulated 143 ± 2 γH2AX foci on an average per cell after 1 h of irradiation, which were reduced to 61 ± 1 (a reduction by 58%) due to the intervention of CpL-S. The CpL-B also showed

Fig. 2. The two fractions of CpL scavenge ROS in normal cell lines. COS-7 and HaCat cells were grown on cover slips and treated with 20 μg of CpL. After 24 h, the cells were treated with CellROX® green and NucBlue™ for 30 min. Then the cells were irradiated with 0 or 10 Gy. Immediately after irradiation, the cells were fixed with paraformaldehyde and were mounted on slides for fluorescence microscopic observations. Fluorescence intensities of at least 50 cells from each group were measured by ImageJ. Representative micrographs of COS-7 cells (A), HaCat cells (B), randomly captured by confocal microscope; graphical representation of fluorescence intensities of COS-7 cells (C) and HaCat cells (D), measured by ImageJ. Bar columns represent average of 3 experiments (the data has been normalized to control) and error bars represent ± standard error of means. p-Values of statistically significant differences are shown. **$p < 0.005$, ***$p < 0.0005$, ****$p < 0.0001$.

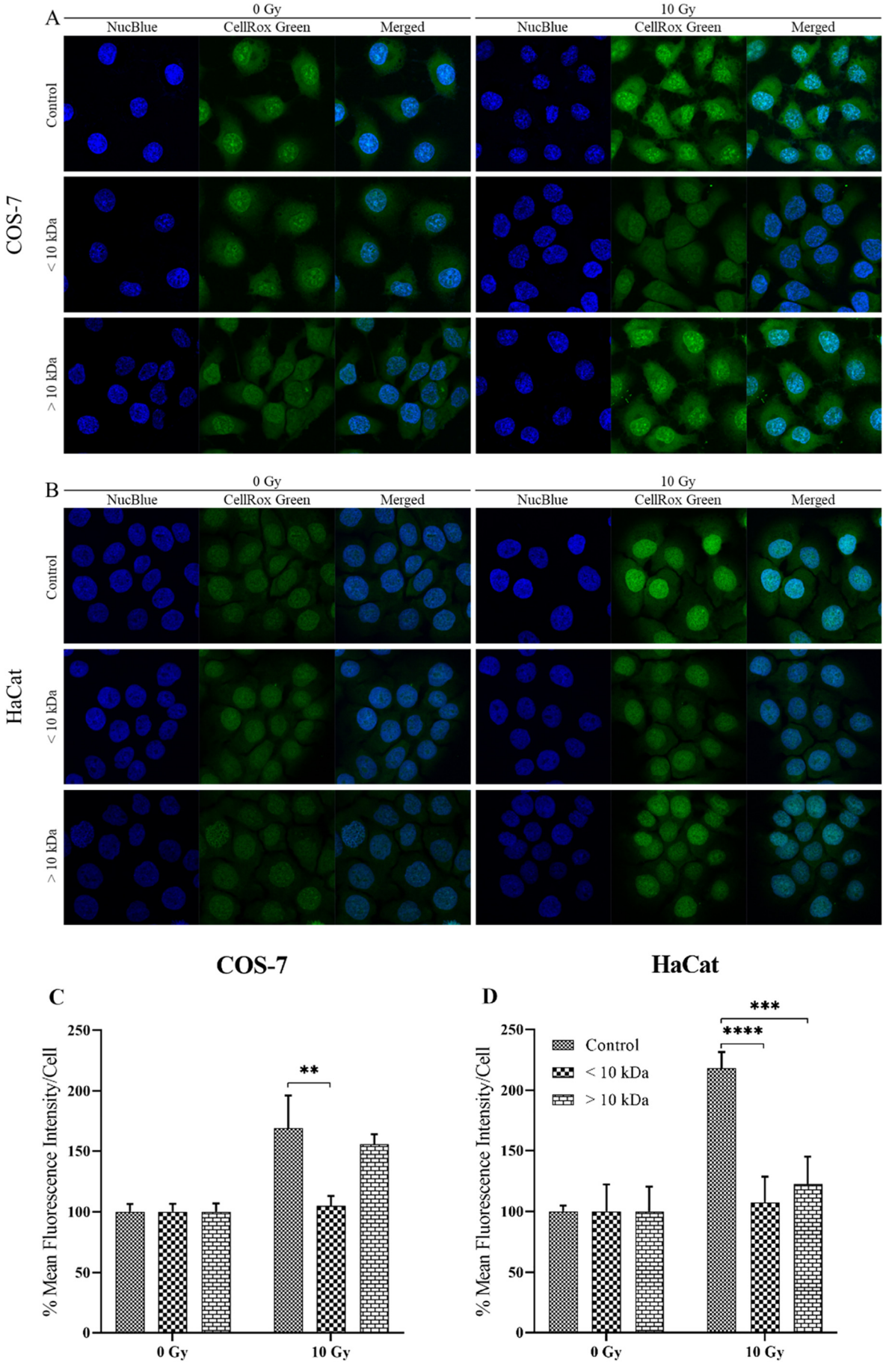
A
0 Gy
10 Gy
NucBlue
CellRox Green
Merged
Control
< 10 kDa
> 10 kDa
COS-7
B
HaCat
C
COS-7
% Mean Fluorescence Intensity/Cell
250
200
150
100
50
0
**
0 Gy
10 Gy
D
HaCat
***
****
Control
< 10 kDa
> 10 kDa

radioprotective effects by preventing 24.5% DSBs (143 foci ± 2 vs 108 ± 3). When the cells were allowed to grow for 24 h post-IR, 42% (82 ± 2) of DSBs were repaired by the cells in the 10 Gy group. However, even at 24 h, it was evident that the CpL-S protected from radiation-induced DNA damage by preventing 55% (37 ± 1) DSBs, while the CpL-B prevented only 21% (65 ± 2) DSBs as revealed by γH2AX foci counting. Similarly, in HaCat cells (Fig. 3D), on an average 153 ± 4 γH2AX foci per cell were formed at the DSBs, which were reduced to 87 ± 9 (a reduction by 43.2%) in the CpL-S treated cells and 144 foci ± 12 (a decrease of 5.9%) 1 h post-IR. At 24 h post-IR, HaCat cells had repaired 35.3% DSBs, as evident by the reduction in γH2AX foci (99 ± 23). These foci reduced faster in the CpL-S treated group (60 ± 6); however, CpL-B treated group didn't show any significant change in the number of γH2AX foci (96 ± 13).

3.4. CpL reduces the expression of homologous repair marker Rad51

IR-exposed cells have higher expression of Rad51, which were reduced in the CpL treated cells at 3 h and 24 h post-IR. A basal level expression of Rad51 can also be visualized in the un-irradiated cells (Fig. 4A and B), which can be attributed to the normal functioning of cells. It was found that the COS-7 cells (Fig. 4C), exposed to 10 Gy IR, have accumulated 62.1 ± 1.1 Rad51 foci on an average per cell after 3 h of irradiation, which were reduced to 30.3 ± 1.1 (a reduction by 51.2%) in the CpL-S treated group. The CpL-B also showed 23.3% reduced foci (47.6 ± 1.2). When the cells were allowed to grow for 24 h post-IR, 64.7% of DSBs were repaired by the cells in the 10 Gy group. However, even at 24 h, it was evident that the CpL-S treated groups had 39.3% more foci repaired (21.9 ± 0.57 vs 13.3 ± 0.4), while in the CpL-B,

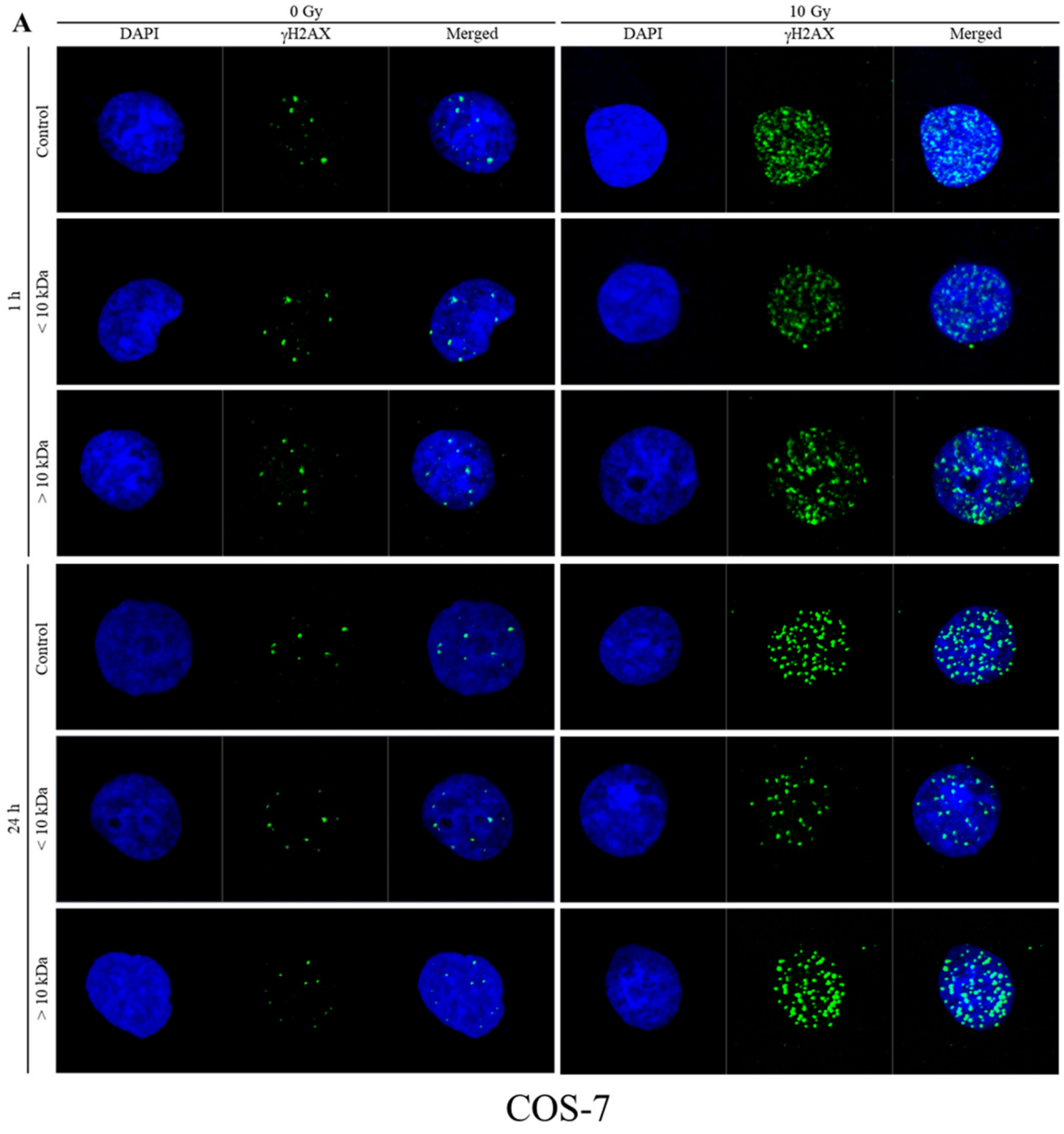

Fig. 3. CpL treated cells show reduced expression of DNA damage marker γH2AX. Cells were treated with 0 or 20 μg of CpL for 24 h and irradiated with 0 or 10 Gy. Samples were collected at 1 h and 24 h post–irradiation and fixed with paraformaldehyde. For the detection of DSBs, the cells were stained with anti-γH2AX antibodies and Alexafluor 488 conjugated secondary antibodies, while nucleus was counter-stained with DAPI. Random images from each group were captured by confocal microscope (LSM-880, Zeiss). Representative micrographs of γH2AX expression at 1 & 24 h post-irradiation in COS-7 (A) and HaCat (B). Graphical representation of average γH2AX foci per cell in COS-7 (C) and HaCat (D), counted by CellProfiler, in at least 50 cells from each group. Columns represent average number of foci per cell and the error bars represent ± standard error of means. p-Values of statistically significant differences are shown. *$p < 0.05$; **$p < 0.005$; ***$p < 0.0001$.

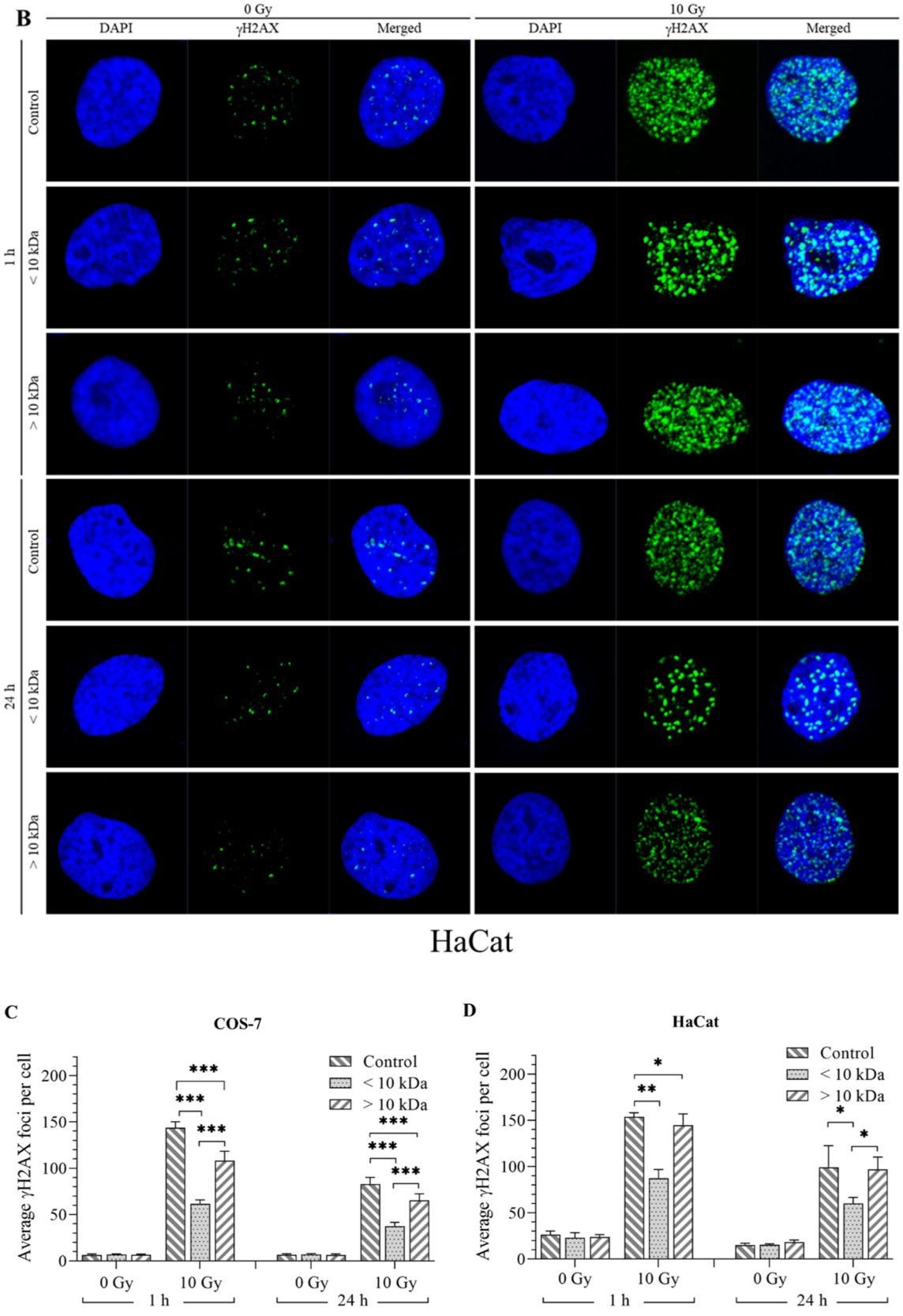

Fig. 3 (*continued*).

only 16.2% more foci were reduced (82 ± 2 vs 65 ± 2). Similarly, in HaCat cells, 3 h post-IR (Fig. 4D) on an average 69.6 ± 0.9 Rad51 foci per cell were formed, which were prevented by 60.1% (27.3 ± 9.8) in the CpL-S treated cells and 23.9% (52.9 ± 10.3) in the CpL-B treated group. After 24 h of irradiation, HaCat cells had reduced 42.7% foci (39.9 ± 6.4). These foci decreased by 53.9% in the CpL-S treated group (18.4 ± 2.6), whereas CpL-B treated group repaired only 29.6% more foci (28.1 ± 2.9).

3.5. CpL reduces the expression of non-homologous end-joining repair marker pDNA-PKcs

It was observed that the IR exposed cells have higher expression of pDNA-PKcs, which were reduced in the CpL treated cells at 1 h as well as 24 h post-IR. In addition to radiation-induced expression of pDNA-PKcs, a basal level of pDNA-PKcs foci can also be visualized in un-irradiated cells (Fig. 5A and B). It was seen that after 1 h, in the COS-7 cells (Fig. 5C) irradiated with 10 Gy, 82.2 ± 2.9 pDNA-PKcs foci were formed per cell, which were reduced to 44.5 ± 2.2 (a reduction of 45.8%) due to the treatment of CpL-S. The CpL-B also reduced the foci by 21.8% (64.7 ± 2.5). When the cells were allowed to grow for 24 h post-IR, 70.9% of foci were reduced (23.9 ± 0.7). Additionally, the CpL-S extended foci reduction by 32.4% more than the control group (16.1 ± 0.7), while the CpL-B could reduce only 14.6% foci (20.4 ± 0.7). On the other hand, in HaCat cells (Fig. 5D), 1 h post-IR, on an average 75.0 ± 2.3 pDNA-PKcs foci were formed per cell, which were reduced to 32.1 ± 1.7 (a reduction by 57.3%) in the CpL-S treated cells and 57.7 foci ± 1.6 (a decrease of 23.1%) in the CpL-B treated group. At 24 h post-IR, 52.9% of pDNA-PKcs foci were reduced (39.7 ± 1.3). These foci were reduced more in the CpL-S treated group by 53.1% of control in the same time frame (18.6 ± 0.9). The CpL-B treated group showed slightly lower reduction as only 26.2% foci were reduced as compared to control (29.3 ± 1.8).

3.6. CpL reduces the expression of DNA damage marker (γH2AX) in the 3D skin tissue

After in vitro testing of CpL for its radioprotective ability, we subjected CpL for in vivo radioprotective evaluation. Like normal cell

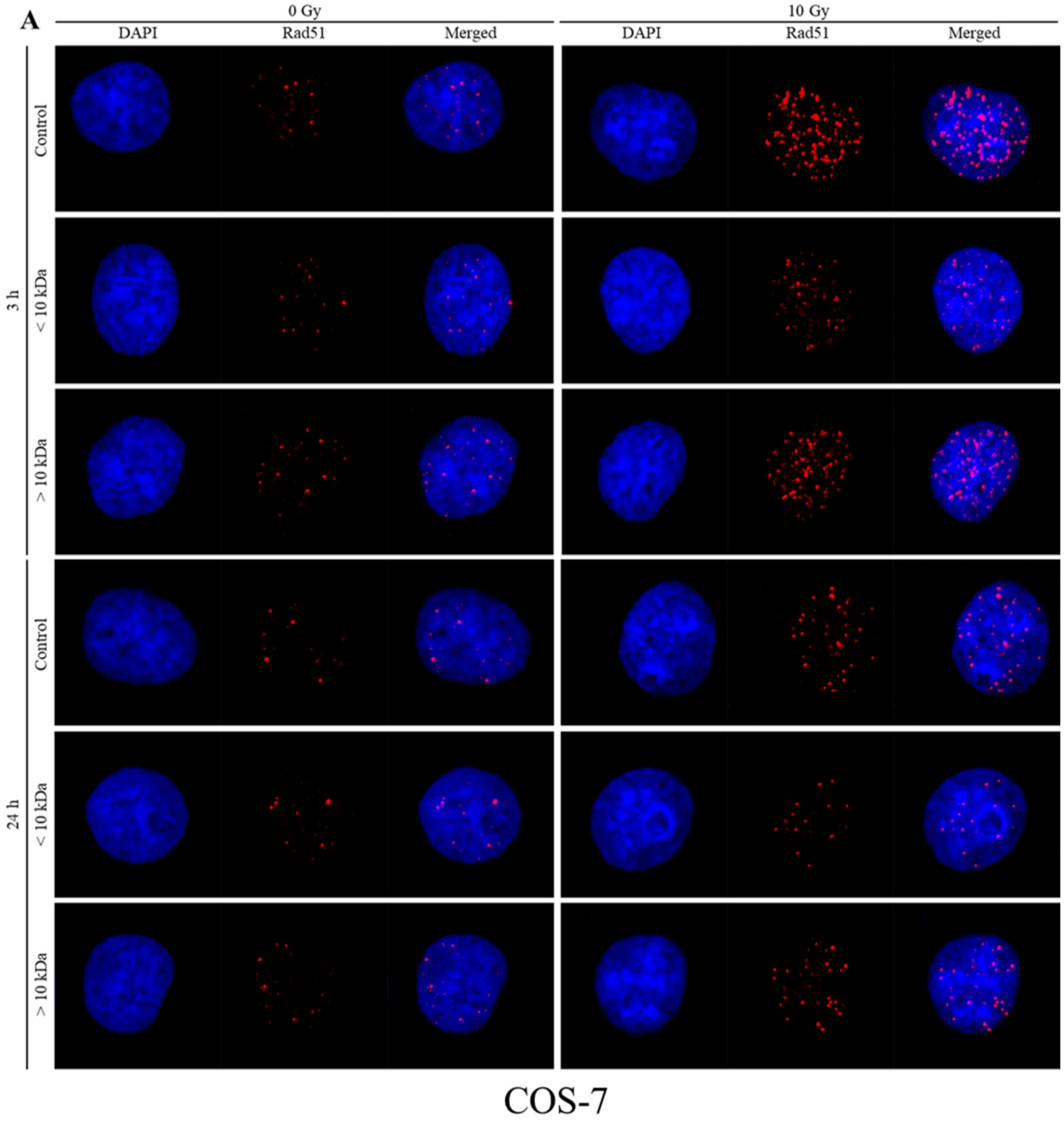

Fig. 4. CpL treated cells show reduced expression of homologous DNA repair marker (Rad51). Cells were treated with 0 or 20 μg of CpL for 24 h and irradiated with 0 or 10 Gy. Samples were collected at 3 h and 24 h post–irradiation and fixed with paraformaldehyde. For the detection of DNA HR foci, the cells were stained with anti-Rad51 antibodies and Alexafluor 594 conjugated secondary antibodies, while nucleus was stained with DAPI. Random images from each group were captured by confocal microscope (LSM-880, Zeiss). Representative micrographs of Rad51 expression at 3 & 24 h post-irradiation in COS-7 (A) and HaCat (B). Graphical representation of average Rad51 foci per cell in COS-7 (C) and HaCat (D), counted by CellProfiler, in at least 50 cells from each group. Bars represent average number of foci per cell and the error bars represent ± standard error of means. p-Values of statistically significant differences are shown. *$p < 0.05$; **$p < 0.005$; ***$p < 0.0001$.

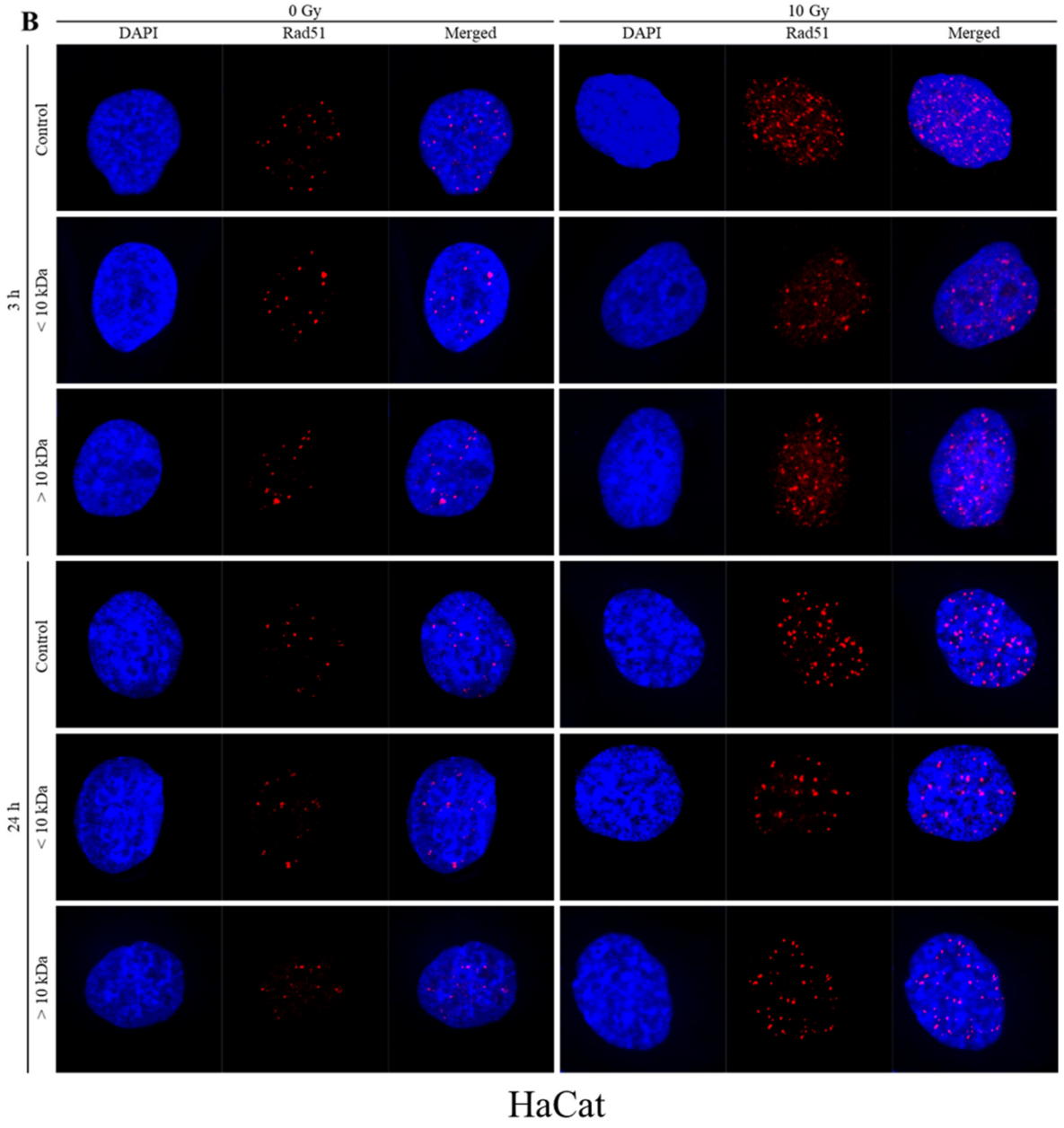

Fig. 4 (*continued*).

lines, the 3D skin tissues didn't show any significant toxicity, as seen in the H&E stained sections, and the cells appeared normal (Fig. 6A). In the control group, all the cells were seen to have expressed γH2AX (173.7/173.7). The IR + CpL treated sections show lower expression of γH2AX compared to IR only group, which suggests that CpL extended its radioprotection to the 3D skin tissues. It can be seen that 1 h post-IR, CpL-S treated tissue sections show only 69.7% ± 1.3 (90.7/130) cells positive for γH2AX expression (Fig. 6B and C), while the CpL-B treated tissue sections have 91.4% ± 2.5 (128/140) positive cells for γH2AX expression. After 24 h post-IR, 47.3% of irradiated cells repaired DNA damage by themselves. However, CpL-S treated cells had a higher rate of repair as shown by the reduction of 69.9% ± 1.3 γH2AX positive cells, while the CpL-B still had 46.4% ± 2.3 (54/116.3) γH2AX positive cells compared to control. These findings confirm that the CpL-S has a better radio-protection ability than CpL-B at 1 h and 24 h post-IR.

4. Discussion

We have shown radioprotective effects of CpL in the normal cells by MTT assay, ROS assay, and estimating DNA damage repair (γH2AX, Rad51, pDNA-PKcs) by immunofluorescence. Further, we evaluated DNA damage in 3D skin tissues by counting the cells positive for γH2AX expression. It was evident that CpL-S imparted significantly better radioprotection to the normal cell in culture and 3D skin tissues.

It is estimated that in a cell usually 50 DSBs can occur per cell cycle, however, if eukaryotic and bacterial cells express a functional DNA repair system, they can survive numerous DSBs [24]. Significant damage to cellular structures transpires when IR-induced generation of free radicals out-paces the cell's ability to neutralize these highly reactive moieties [15]. In radiation biology, clonogenic assay is a preferred method in which the capacity of cells' reproductive viability is evaluated. Based on

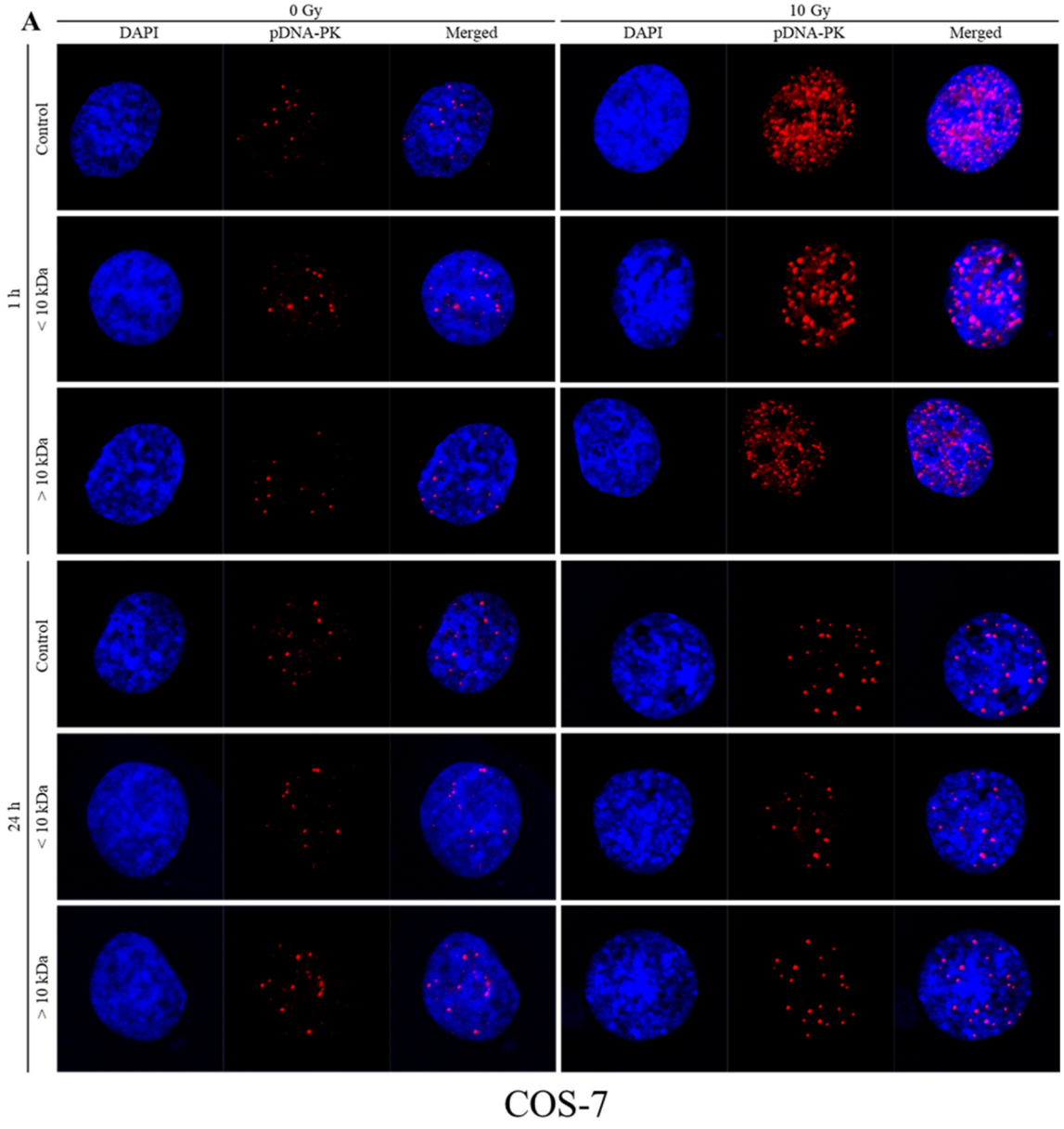

Fig. 5. CpL treated cells show reduced expression of NHEJ DNA repair marker (pDNA-PKcs). Cells were treated with 0 or 20 μg of CpL for 24 h and irradiated with 0 or 10 Gy. Samples were collected at 1 h and 24 h post–irradiation and fixed with paraformaldehyde. For the detection of DNA NHEJ foci, the cells were stained with anti-pDNA-PKcs antibodies and Alexafluor 594 conjugated secondary antibodies, while nucleus was stained with DAPI. Random images from each group were captured by confocal microscope (LSM-880, Zeiss). Representative micrographs of Rad51 expression at 1 & 24 h post-irradiation in COS-7 (A) and HaCat (B). Graphical representation of average pDNA-PKcs foci per cell in COS-7 (C) and HaCat (D), counted by CellProfiler, in at least 50 cells from each group. Bars represent average number of foci per cell and the error bars represent ± standard error of means. p-Values of statistically significant differences are shown. $^{**}p < 0.005$; $^{***}p < 0.0001$.

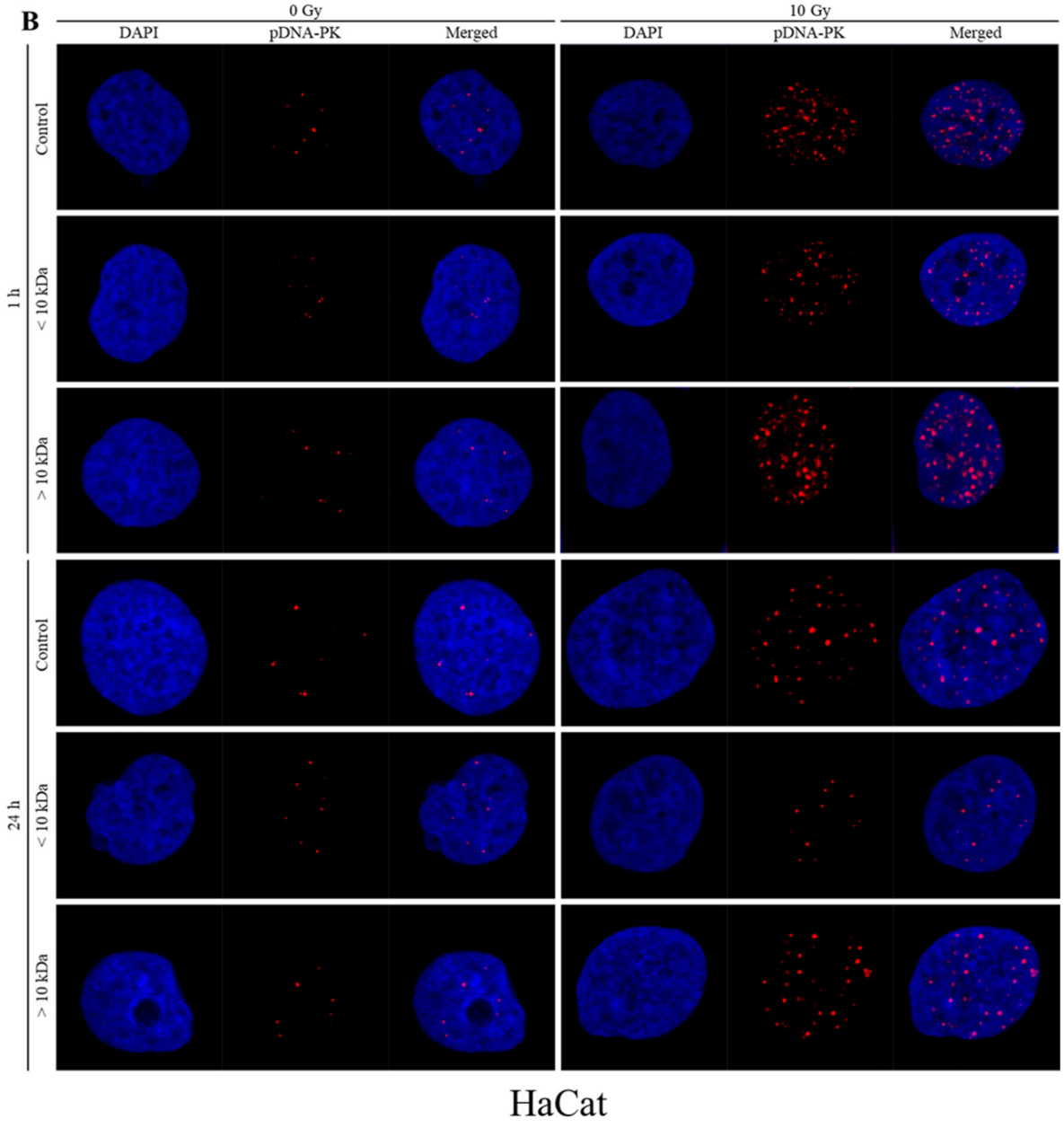

Fig. 5 (*continued*).

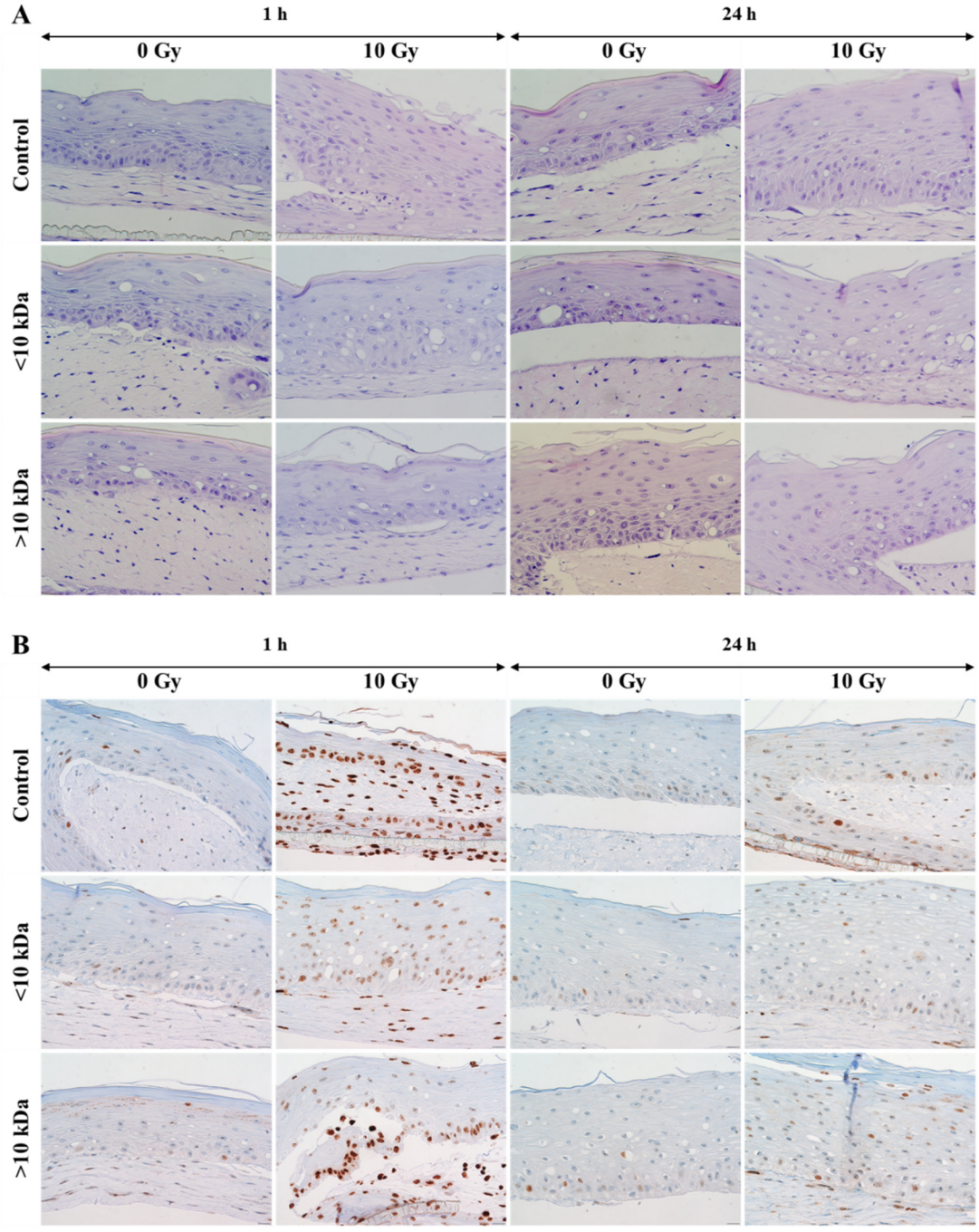
A
1 h
24 h
0 Gy
10 Gy
0 Gy
10 Gy
Control
<10 kDa
>10 kDa
B
1 h
24 h
0 Gy
10 Gy
0 Gy
10 Gy
Control
<10 kDa
>10 kDa

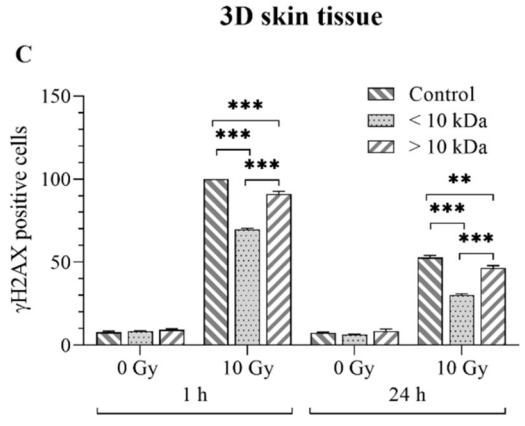
3D skin tissue
C
γH2AX positive cells
150
100
50
0
Control
< 10 kDa
> 10 kDa
***
***
***
**
***
***
0 Gy
10 Gy
0 Gy
10 Gy
1 h
24 h

the fact that MTT reduction to formazan is proportional to the number of metabolically active cells in culture, MTT assay is one of the most popular methods when the rapid estimation of cell proliferation and viability is desired [25,26]. In the present study, MTT assay revealed that both the normal cell lines were protected from the radiation-induced injury, expressed as higher cell viability in CpL + IR treated cells against IR only cells.

ROS are the by-products of metabolism, and these highly reactive molecules can oxidize various biomolecules leading to severe cell damage or death. Thus, we chose to evaluate ROS levels' change in CpL treated cells by fluorescence microscopy using a fluorogenic and fixable probe, CellROX® green. Cells exposed to 10 Gy IR show increased fluorescence compared to control groups in both the cell lines. Treatment of cells under oxidative stress with CpL resulted in diminished staining with CellROX® green, demonstrating the high ROS scavenging potential of CpL. The confocal images captured randomly and analyzed by ImageJ software show a significant reduction of ROS by CpL in both the cell lines. Li et al. and Lee et al. have reported earlier that short peptides with 2–10 amino acids demonstrate much better antioxidant activities than their parent native proteins or large polypeptides [27,28]. Among amino acids, tyrosine, tryptophan, methionine, histidine, cysteine and phenylalanine exhibit the highest antioxidant activity in decreasing order [29]. The antioxidant peptides possess metal chelation or hydrogen or electron-donating properties, which help in interaction with free radicals leading to the termination of free radical chain reaction, subsequently protecting the cells from severe damage [30,31].

The introduction of DNA DSBs activates a complex set of responses in eukaryotic cells, including cell cycle arrest, DNA repair factors relocalization, and apoptosis in some cases. Many researchers have previously demonstrated that on an average, 20 γH2AX foci per Gy per cell were formed, 30 min post-IR [32]. Loss of these γH2AX foci has been proposed to reflect the DNA repair of the DSBs [33]. This study has shown that the foci numbers were maximum at 1 h in irradiated cells but were significantly lower in CpL treated cells. These foci further decreased at 24 h, and remarkably lower in the CpL treated groups, especially in the CpL-S treated cells, where these foci were always lower than the CpL-B treated cells. These results signify the potential of CpL-S to protect the cell lines from radiation-induced injury.

In mammalian cells, DSBs are repaired via 2 main pathways, homologous recombination (HR) and non-homologous end-joining (NHEJ) [34,35]. HR is considered to be an accurate DSB repair pathway, mostly active during S and G2 phases when a duplicate sister chromatid, produced during the S phase, is available to be used as a template [36]. As most of the cells in human body are in the G1 or G0 stage (where the HR is suppressed), NHEJ is the pathway that will repair the majority of IR-induced DSBs. It has been reported that the components of the DNA damage repair system like BRCA1, 53BP1, MC1, RAD51, MRE11/RAD50/NBS1 complex, lead to the formation of IR-induced foci which localize at the site of γH2AX foci [37]. At 1 h and a prolonged time of 24 h post-IR, the cells treated with CpL have shown the loss of γH2AX along with Rad51 and pDNA-PKcs foci, suggesting repair of the DSBs.

In the 3D skin model (Fig. 6A), we didn't observe any morphological changes post-IR (10 Gy), as we checked the sections at 1 h and 24 h following 10 Gy irradiation, which seems to be a short time to visualize and evaluate histological differences like epidermal thickness, density of basal cells and density of epithelial cells, etc. However, we did find significant changes at the molecular level. The number of γH2AX expressing cells in 10 Gy irradiated sections, were seen to be highest at 100%, as all the cells got stained with γH2AX, which were gradually reduced with time and in the section treated with CpL, more so in the CpL-S treated sections. The reduction of γH2AX positive cells in CpL treated sections confirms the radioprotection ability of CpL.

In the CpL-B fraction, there are several ROS scavenging enzymes present like superoxide dismutase, thioredoxin peroxidase, glutathione peroxidase, etc. (cryptodb.org). Lee et al. have reported previously that following 10 kGy IR, thioredoxin peroxidase-like protein (TPx; 22 kDa), was highly upregulated in Cp oocysts [38]. Later, Yoon et al. found that the recombinant TPx from Cp (CpTPx) had higher antioxidant activity as compared to TPx from *C. muris* (CmTPx), which is radio-sensitive [39]. Further, Hong et al. demonstrated that expression of CpTPx in COS-7 cells conferred radioprotection from up to 8 Gy of IR [8]. However, in the present study, we found that CpL-S had better radioprotective activity compared to CpL-B, in terms of cell viability, ROS scavenging activity and expression of DNA damage repair markers. There are 2 methods for the internalization of macromolecules. One is endocytosis, and the other is more specific receptor-ligand mediated endocytosis. However, the process of cellular uptake is limited by the size of the macromolecules, as membrane permeability drops-off steeply at molecular weights above 1 kDa [40]. Hence, we think that even though the CpL-B is believed to be rich in antioxidant enzymes/molecules, their uptake is compromised in normal cellular conditions. In the CpL-S, plenty of free and structural amino acids seem to be present along with very short peptides, which are well known to scavenge ROS efficiently. Additionally, the proteasome and ubiquitin associated components are highly activated in *C. parvum*, inferring that the oocysts might engage protein degradation pathways to overcome its incapability of amino acid synthesis. *C. parvum* dedicates substantial resources to the gene expression and synthesis, modification and degradation of proteins. Bearing in mind the incompetence of *C. parvum* to synthesize any nutrients *de novo*, including amino acids, it is believed that the parasite banks heavily on protein degradation pathways to recycle amino acids. In this fashion, the environmental oocysts (deprived of nutrients from host cells) maintain a protein synthetic capacity [41]. Through the *C. parvum* protein database (cryptodb.org), we checked the list of proteins present in both the fractions and found that 2 ubiquitin-like small proteins (EAZ51324.1, 73 amino acids; EAZ51602.1, 78 amino acids) may be present in the CpL-S. We propose the 2 ubiquitin-like proteins might be of significant help to the cells in vitro and in vivo to carry out protein recycling in response to IR-related stress. Thus the large pool of small molecules in the CpL-S treated cells helps to scavenge ROS more effectively than the CpL-B and subsequently provides better radioprotection.

5. Summary & conclusion

We prepared two fractions from CpL, based on molecule size of less than 10 kDa or more than 10 kDa and analyzed their radioprotective potential on normal cells and 3D skin tissue by evaluating the DNA damage repair markers and ROS scavenging ability. To the best of our knowledge, this is the first report on the radioprotective effects of CpL on normal cells and 3D skin tissues. The intervention of CpL significantly improved cell viability of normal cell lines irradiated up to 10 Gy. Also, the CpL effectively scavenged ROS in both the normal cell lines when compared with the control group. Both the findings were further confirmed by the DNA damage and repair markers γH2AX, Rad51, and pDNA-PKcs expression, which were significantly reduced in irradiated cells treated with CpL suggesting that the CpL protected DNA from the radiation-induced damage. Higher rescue of normal cells and 3D skin tissue by CpL-S compared to CpL-B or control group demonstrates the radioprotective potential of CpL-S. Our results present the necessary

Fig. 6. γH2AX expression is reduced in CpL treated 3D skin sections (NeoDerm®ED). The 3D skin tissue samples were treated with 0 or 40 μg of CpL for 24 h. Then the tissues were irradiated with 0 or 10 Gy IR. Tissue samples were collected after 1 and 24 h post-irradiation. Tissues were fixed with formalin and embedded in paraffin. 4-μm thick sections were mounted on silanized slides and were stained with H&E (A) or γH2AX (B). Black bar = 20 μm. Graphical representation of γH2AX positive cells in the 3D skin model (C), counted manually from 3 sections each having more than 100 cells. Bars represent γ H2AX positive cells in percent, while error bars represent ± standard deviation. p-Values of statistically significant differences are shown. $^{**}p < 0.005$; $^{***}p < 0.0001$.

prelude for future efforts towards a promising radioprotector development. Further studies are warranted to identify and exploit the full potential of CpL-S bioactive components responsible for the radioprotection and test their efficacy in pre- or post-exposure settings.

Supplementary data to this article can be found online at https://doi.org/10.1016/j.ijbiomac.2021.02.151.

CRediT authorship contribution statement

Pankaj Kumar Chaturvedi: conceptualization, methodology, investigation, formal analysis, writing - original draft, writing - review editing

Enkhsaikhan Erdenetuya: investigation
Prabakaran D.S.: investigation
Chang-Gok Woo: investigation
Ki-Hwan Kim: methodology, writing – review and editing
Jae-Ran Yu: methodology, project administration, writing – review and editing
Woo-Yoon Park: conceptualization, supervision, validation, writing - review and editing, project administration, resources, funding acquisition.

Declaration of competing interest

The authors have no conflict of interest to declare.

Acknowledgements

This study was supported by the Ministry of Science and ICT, South Korea; and by the National Research Foundation (NRF) of Korea (NRF-2016M2A2A7A03913699, 2013M7A1A1075764).

References

[1] R.M. Johnke, J.A. Sattler, R.R. Allison, Radioprotective agents for radiation therapy: future trends, Futur. Oncol. (London, England) 10 (15) (2014) 2345–2357, https://doi.org/10.2217/fon.14.175.

[2] E.J. Hall, A.J. Giaccia, Molecular mechanisms of DNA and chromosome damage and repair. In: Radiobiology for the Radiologist (7th Edition), Wolters Kluwer Health/Lippincott Williams & Wilkins, Philadelphia, 2012.

[3] M.I. Koukourakis, Radiation damage and radioprotectants: new concepts in the era of molecular medicine, Br. J. Radiol. 85 (1012) (2012) 313–330, https://doi.org/10.1259/bjr/16386034.

[4] M.H. Andersen, J.C. Becker, P. Straten, Regulators of apoptosis: suitable targets for immune therapy of cancer, Nat. Rev. Drug Discov. 4 (5) (2005) 399–409, https://doi.org/10.1038/nrd1717.

[5] J.A. Downs, N.F. Lowndes, S.P. Jackson, A role for *Saccharomyces cerevisiae* histone H2A in DNA repair, Nature 408 (6815) (2000) 1001–1004, https://doi.org/10.1038/35050000.

[6] J. Fillingham, M.C. Keogh, N.J. Krogan, GammaH2AX and its role in DNA double-strand break repair, Biochem. Cell Biol. 84 (4) (2006) 568–577, https://doi.org/10.1139/o06-072.

[7] E.P. Rogakou, D.R. Pilch, A.H. Orr, V.S. Ivanova, W.M. Bonner, DNA double-stranded breaks induce histone H2AX phosphorylation on serine 139, J. Biol. Chem. 273 (10) (1998) 5858–5868, https://doi.org/10.1074/jbc.273.10.5858.

[8] S. Hong, J.H. Kim, S. Yoon, K. Kim, S. Sim, W.Y. Park, J.R. Yu, Expression of *Cryptosporidium parvum* thioredoxin peroxidase in COS-7 cells confers radioprotection, Exp. Parasitol. 163 (2016) 8–15, https://doi.org/10.1016/j.exppara.2016.01.012.

[9] S. Pizzimenti, C. Toaldo, P. Pettazzoni, M.U. Dianzani, G. Barrera, The "two-faced" effects of reactive oxygen species and the lipid peroxidation product 4-hydroxynonenal in the hallmarks of cancer, Cancers (Basel) 2 (2) (2010) 338–363, https://doi.org/10.3390/cancers2020338.

[10] C.C. Yeh, J.Z. Chang, W.H. Yang, H.H. Chang, E.H. Lai, M.Y. Kuo, NADPH oxidase 4 is involved in the triethylene glycol dimethacrylate-induced reactive oxygen species and apoptosis in human embryonic palatal mesenchymal and dental pulp cells, Clin. Oral Investig. 19 (6) (2015) 1463–1471, https://doi.org/10.1007/s00784-014-1370-7.

[11] S. Elmore, Apoptosis: a review of programmed cell death, Toxicol. Pathol. 35 (4) (2007) 495–516, https://doi.org/10.1080/01926230701320337.

[12] M. Podhorecka, A. Skladanowski, P. Bozko, H2AX phosphorylation: its role in DNA damage response and cancer therapy, J. Nucleic Acids 2010 (2010)https://doi.org/10.4061/2010/920161.

[13] M.A. Kuefner, M. Brand, C. Engert, S.A. Schwab, M. Uder, Radiation induced DNA double-strand breaks in radiology, Rofo 187 (10) (2015) 872–878, https://doi.org/10.1055/s-0035-1553209.

[14] J.A. Brink, J.D. Boice Jr., Science to practice: can antioxidant supplements protect against the possible harmful effects of ionizing radiation from medical imaging? Radiology 264 (1) (2012) 1–2, https://doi.org/10.1148/radiol.12120712.

[15] T.A. Smith, D.R. Kirkpatrick, S. Smith, T.K. Smith, T. Pearson, A. Kailasam, K.Z. Herrmann, J. Schubert, D.K. Agrawal, Radioprotective agents to prevent cellular damage due to ionizing radiation, J. Transl. Med. 15 (1) (2017), 232, https://doi.org/10.1186/s12967-017-1338-x.

[16] V. Kuruba, P. Gollapalli, Natural radioprotectors and their impact on cancer drug discovery, Radiat. Oncol. J. 36 (4) (2018) 265–275, https://doi.org/10.3857/roj.2018.00381.

[17] M.J. Daly, E.K. Gaidamakova, V.Y. Matrosova, J.G. Kiang, R. Fukumoto, D.Y. Lee, N.B. Wehr, G.A. Viteri, B.S. Berlett, R.L. Levine, Small-molecule antioxidant proteome-shields in *Deinococcus radiodurans*, PLoS One 5 (9) (2010), e12570, https://doi.org/10.1371/journal.pone.0012570.

[18] P. Gupta, M. Gayen, J.T. Smith, E.K. Gaidamakova, V.Y. Matrosova, O. Grichenko, B. Knollmann-Ritschel, M.J. Daly, J.G. Kiang, R.K. Maheshwari, MDP: a *Deinococcus* Mn2+-decapeptide complex protects mice from ionizing radiation, PLoS One 11 (8) (2016), e0160575, https://doi.org/10.1371/journal.pone.0160575.

[19] E.K. Gaidamakova, I.A. Myles, D.P. McDaniel, C.J. Fowler, P.A. Valdez, S. Naik, M. Gayen, P. Gupta, A. Sharma, P.J. Glass, R.K. Maheshwari, S.K. Datta, M.J. Daly, Preserving immunogenicity of lethally irradiated viral and bacterial vaccine epitopes using a radio- protective Mn2+-peptide complex from *Deinococcus*, Cell Host Microbe 12 (1) (2012) 117–124, https://doi.org/10.1016/j.chom.2012.05.011.

[20] M. Bouzid, P.R. Hunter, R.M. Chalmers, K.M. Tyler, *Cryptosporidium* pathogenicity and virulence, Clin. Microbiol. Rev. 26 (1) (2013) 115–134, https://doi.org/10.1128/CMR.00076-12.

[21] J.R. Yu, W.Y. Park, The effect of gamma-irradiation on the viability of *Cryptosporidium parvum*, J. Parasitol. 89 (3) (2003) 639–642, https://doi.org/10.1645/0022-3395(2003)089[0639:TEOIOT]2.0.CO;2.

[22] M.A.G. Morales, C.M. Ausiello, F. Urbani, E. Pozio, Crude extract and recombinant protein of *Cryptosporidium parvum* oocysts induce proliferation of human peripheral blood mononuclear cells in vitro, J. Infect. Dis. 172 (1) (1995) 211–216www.jstor.org/stable/30135481.

[23] C. McQuin, A. Goodman, V. Chernyshev, L. Kamentsky, B.A. Cimini, K.W. Karhohs, M. Doan, L. Ding, S.M. Rafelski, D. Thirstrup, W. Wiegraebe, S. Singh, T. Becker, J.C. Caicedo, A.E. Carpenter, CellProfiler 3.0: next-generation image processing for biology, PLoS Biol. 16 (7) (2018), e2005970, https://doi.org/10.1371/journal.pbio.2005970.

[24] M.M. Vilenchik, A.G. Knudson, Radiation dose-rate effects, endogenous DNA damage, and signaling resonance, Proc. Natl. Acad. Sci. U. S. A. 103 (47) (2006) 17874–17879, https://doi.org/10.1073/pnas.0607995103.

[25] T. Mosmann, Rapid colorimetric assay for cellular growth and survival: application to proliferation and cytotoxicity assays, J. Immunol. Methods 65 (1–2) (1983) 55–63, https://doi.org/10.1016/0022-1759(83)90303-4.

[26] Y. Rai, R. Pathak, N. Kumari, D.K. Sah, S. Pandey, N. Kalra, R. Soni, B.S. Dwarakanath, A.N. Bhatt, Mitochondrial biogenesis and metabolic hyperactivation limits the application of MTT assay in the estimation of radiation induced growth inhibition, Sci. Rep. 8 (1) (2018), 1531, https://doi.org/10.1038/s41598-018-19930-w.

[27] B. Li, F. Chen, X. Wang, B. Ji, Y. Wu, Isolation and identification of antioxidative peptides from porcine collagen hydrolysate by consecutive chromatography and electrospray ionization–mass spectrometry, Food Chem. 102 (4) (2007) 1135–1143, https://doi.org/10.1016/j.foodchem.2006.07.002.

[28] J.K. Lee, H.-G. Byun, Characterization of antioxidative peptide purified from black eelpout (*Lycodes diapterus*) hydrolysate, Fish. Aquat. Sci. 22 (1) (2019), 22, https://doi.org/10.1186/s41240-019-0137-0.

[29] A. Davalos, M. Miguel, B. Bartolome, R. Lopez-Fandino, Antioxidant activity of peptides derived from egg white proteins by enzymatic hydrolysis, J. Food Prot. 67 (9) (2004) 1939–1944, https://doi.org/10.4315/0362-028x-67.9.1939.

[30] J. Ren, M. Zhao, J. Shi, J. Wang, Y. Jiang, C. Cui, Y. Kakuda, S.J. Xue, Purification and identification of antioxidant peptides from grass carp muscle hydrolysates by consecutive chromatography and electrospray ionization-mass spectrometry, Food Chem. 108 (2) (2008) 727–736, https://doi.org/10.1016/j.foodchem.2007.11.010.

[31] L. You, M. Zhao, J.M. Regenstein, J. Ren, Purification and identification of antioxidative peptides from loach (*Misgurnus anguillicaudatus*) protein hydrolysate by consecutive chromatography and electrospray ionization-mass spectrometry, Food Res. Int. 43 (4) (2010) 1167–1173, https://doi.org/10.1016/j.foodres.2010.02.009.

[32] B. Rydberg, Radiation-induced heat-labile sites that convert into DNA double-strand breaks, Radiat. Res. 153 (6) (2000) 805–812, https://doi.org/10.1667/0033-7587(2000)153[0805:rihlst]2.0.co;2.

[33] K. Rothkamm, M. Lobrich, Evidence for a lack of DNA double-strand break repair in human cells exposed to very low x-ray doses, Proc. Natl. Acad. Sci. U. S. A. 100 (9) (2003) 5057–5062, https://doi.org/10.1073/pnas.0830918100.

[34] E. Mladenov, G. Iliakis, Induction and repair of DNA double strand breaks: the increasing spectrum of non-homologous end joining pathways, Mutat. Res. 711 (1–2) (2011) 61–72, https://doi.org/10.1016/j.mrfmmm.2011.02.005.

[35] B.L. Mahaney, K. Meek, S.P. Lees-Miller, Repair of ionizing radiation-induced DNA double-strand breaks by non-homologous end-joining, Biochem. J. 417 (3) (2009) 639–650, https://doi.org/10.1042/BJ20080413.

[36] K. Rothkamm, I. Kruger, L.H. Thompson, M. Lobrich, Pathways of DNA double-strand break repair during the mammalian cell cycle, Mol. Cell. Biol. 23 (16) (2003) 5706–5715, https://doi.org/10.1128/mcb.23.16.5706-5715.2003.

[37] O. Fernandez-Capetillo, A. Lee, M. Nussenzweig, A. Nussenzweig, H2AX: the histone guardian of the genome, DNA Repair (Amst) 3 (8–9) (2004) 959–967, https://doi.org/10.1016/j.dnarep.2004.03.024.

[38] S.-U. Lee, M. Joung, T. Nam, W.-Y. Park, Y.-H. Ji, J.-R. Yu, *Cryptosporidium parvum*: radiation-induced alteration of the oocyst proteome, Exp. Parasitol. 127 (1) (2011) 25–30, https://doi.org/10.1016/j.exppara.2010.06.016.
[39] S. Yoon, W.-Y. Park, J.-R. Yu, Recombinant thioredoxin peroxidase from *Cryptosporidium parvum* has more powerful antioxidant activity than that from *Cryptosporidium muris*, Exp. Parasitol. 131 (3) (2012) 333–338, https://doi.org/10.1016/j.exppara.2012.04.018.
[40] P. Matsson, J. Kihlberg, How big is too big for cell permeability? J. Med. Chem. 60 (5) (2017) 1662–1664, https://doi.org/10.1021/acs.jmedchem.7b00237.
[41] H. Zhang, F. Guo, H. Zhou, G. Zhu, Transcriptome analysis reveals unique metabolic features in the *Cryptosporidium parvum* Oocysts associated with environmental survival and stresses, BMC Genomics 13 (2012) 647, https://doi.org/10.1186/1471-2164-13-647.

Abbreviations

ANOVA: analysis of variance
BRCA1: breast cancer type 1 susceptibility protein
C. muris: Cryptosporidium muris
CmTPx: Cryptosporidium muris thioredoxin peroxidase
Cp: Cryptosporidium parvum
CpL: C. parvum lysate
CpL-B: CpL big fraction (>10 kDa)
CpL-S: CpL small fraction (<10 kDa)
CpTPx: Cryptosporidium parvum thioredoxin peroxidase
D. radiodurans: Deinococcus radiodurans
DAB: 3,3′-diaminobenzidine
DMEM: Dulbecco's Modified Eagle's Medium
DNA: deoxyribonucleic acid
DSBs: double-strand breaks
D-PBS: Dulbecco's PBS
FBS: fetal bovine serum
Gy: gray
h: hour
HEPES: (4-(2-hydroxyethyl)-1-piperazineethanesulfonic acid)
HR: homologous recombination
HRP: horseradish peroxidase
H&E: hematoxylin and eosin
IF: immunofluorescence
IR: ionizing radiation
KCLB: Korean Cell Line Bank
kDa: kilo dalton
LET: linear energy transfer
MDP: Mn^{2+}-decapeptide
MTT: 3-(4,5-dimethylthiazol-2-yl)-2,5-diphenyltetrazolium bromide
MV: mega volt
NHEJ: non-homologous end-joining
NIH: National Institute of Health
PBS: phosphate buffer saline
pDNA-PKcs: phosphorylated DNA dependent protein kinase, catalytic subunit
ROS: reactive oxygen species
RT: radiation therapy
s: seconds
TPx: thioredoxin peroxidase
WST: water soluble tetrazolium
53BP1: tumor suppressor p53-binding protein 1